

Atmospheric Inverse Estimates of Methane Emissions from Central California

Chuanfeng Zhao¹, Arlyn E. Andrews², Laura Bianco^{2,5}, Janusz Eluszkiewicz³, Adam Hirsch^{2,5}, Clinton MacDonald⁴, Thomas Nehrkorn³, Marc L. Fischer¹

¹Environmental Energy Technology Division, Lawrence Berkeley National Lab,
Berkeley, CA, USA

²Earth System Research Laboratory, NOAA, Boulder, CO, USA

³Atmospheric and Environmental Research, Inc., Lexington, MA, USA

⁴Sonoma Technology, Inc., Petaluma, CA, USA

⁵Cooperative Institute for Research in Environmental Sciences, University of
Colorado, Boulder, CO, USA

Abstract. Methane mixing ratios measured at a tall-tower are compared to model predictions to estimate surface emissions of CH₄ in Central California for October-December 2007 using an inverse technique. Predicted CH₄ mixing ratios are calculated based on spatially resolved *a priori* CH₄ emissions and simulated atmospheric trajectories. The atmospheric trajectories, along with surface footprints, are computed using the Weather Research and Forecast (WRF) coupled to the Stochastic Time-Inverted Lagrangian Transport (STILT) model. An uncertainty analysis is performed to provide quantitative uncertainties in estimated CH₄ emissions. Three inverse model estimates of CH₄ emissions are reported. First, linear regressions of modeled and measured CH₄ mixing ratios obtain slopes of 0.73 ± 0.11 and 1.09 ± 0.14 using California specific and Edgar 3.2 emission maps respectively, suggesting that actual CH₄ emissions were about $37 \pm 21\%$ higher than California specific inventory estimates. Second, a Bayesian “source” analysis suggests that livestock emissions are $63 \pm 22\%$ higher than the *a priori* estimates. Third, a Bayesian “region” analysis is carried out for CH₄ emissions from 13 sub-regions, which shows that inventory CH₄ emissions from the Central Valley are underestimated and uncertainties in CH₄ emissions are reduced for sub-regions near the tower site, yielding best estimates of flux from those regions consistent with “source” analysis results. The uncertainty reductions for regions near the tower indicate that a regional network of measurements will be necessary to provide accurate estimates of surface CH₄ emissions for multiple regions.

1. Introduction

Changes in atmospheric methane play an essential role in Earth's climate. CH₄ is now associated with a direct radiative forcing of $\sim 0.48 \text{ Wm}^{-2}$ (IPCC, 2007) and an indirect radiative forcing of $\sim 0.13 \text{ Wm}^{-2}$ [Lelieveld *et al.*, 1998], which accounts for about ½ of the non-CO₂ radiative forcing (0.98 W m^{-2} in 2004) [Hofman *et al.*, 2006] and about ¼ of the total radiative forcing (2.64 W m^{-2} from IPCC 2007) from all greenhouse gases (GHGs). It has been argued that reducing anthropogenic emissions of methane may be an important component of an initial strategy for avoiding the most severe impacts of global warming [Hansen *et al.*, 1998; Hansen, 2004; Shindell *et al.*, 2005]. In particular, reduction of anthropogenic methane emissions may be possible (e.g., improving CH₄ recovery from landfills and waste treatment, reducing industrial emissions, and improving agricultural practices) [Harriss, 1994]. In view of methane's role in the climate system, increased attention has been brought recently to assessing CH₄ sources [Gimson and Uliasz, 2003; Miller *et al.*, 2003; Houweling *et al.*, 2006; Kort *et al.*, 2008].

In California, total GHG emissions in 2004 were approximately 480 MMT CO₂ equivalent, with CH₄ contributing approximately 6 % [CARB, 2007]. Now that California has passed Assembly Bill 32, which requires that greenhouse gases emissions be reduced to 1990 levels by 2020, careful accounting of current CH₄ emissions and of their future reductions is essential. Unfortunately, current inventory and model-based estimates of CH₄ emissions are uncertain because many of the factors controlling emissions are poorly quantified. Atmospheric measurements and inverse modeling may provide an independent method to quantify local to regional CH₄ emissions from California.

Atmospheric inverse methods to estimate the surface CH₄ fluxes from in-situ and
25 remotely sensed CH₄ mixing ratio measurements and modeled wind fields have been
widely applied at both global and regional scales [*Hein et al.*, 1997; *Houweling et al.*,
1999; *Vermeulen et al.*, 1999; *Bergamaschi et al.*, 2000; *Dentener et al.*, 2003; *Gimson
and Uliasz*, 2003; *Manning et al.*, 2003; *Mikaloff Fletcher et al.*, 2004a, b; *Bergamaschi
et al.*, 2005; *Chen and Prinn*, 2006, *Bergamaschi et al.*, 2007; *Kort et al.*, 2008]. In
30 general, the components of atmospheric inverse emission estimates are CH₄ mixing ratio
measurements, an atmospheric transport model (including chemistry for global
simulations), in some cases *a priori* estimates for CH₄ emissions and sinks or their
correlation structure, and a statistical technique to minimize differences between
measured and predicted CH₄ mixing ratios. To estimate CH₄ emissions and their
35 associated uncertainties, errors from each of these components should be accounted for
and formally propagated through the inversion process.

In this study, we employ an approach originally developed to estimate regional CO₂
emissions [*Gerbig et al.*, 2003 a,b] that combines calculation of surface footprints [*Lin et
al.*, 2004] with procedures to estimate transport model uncertainty [*Lin and Gerbig*,
40 2005] using the Stochastic Time-Inverted Lagrangian Transport (STILT) model. Of
particular relevance to our work, *Kort et al.* (2008) recently used observations of CH₄ and
N₂O from an airborne platform in combination with STILT to infer CH₄ and N₂O
emissions from the continental interior of North America in May-June 2003. Our study
also uses STILT, but applies it to a smaller model domain at finer spatial and temporal
45 resolutions, taking advantage of unique computational benefits offered by the Lagrangian
approach.

To address the problem of estimating CH₄ emissions from different sources in Central California, we conducted coordinated CH₄ measurements and modeling as part of the California Greenhouse Gases Emission Measurement (CALGEM) project. Section 2 describes the methods for the measurements of CH₄ mixing ratios, profiler-based estimates of wind fields and boundary layer heights, spatially resolved *a priori* CH₄ emission maps, meteorological transport fields and resulting surface footprints, an analysis of measurement and model errors, and the Bayesian inverse model used to estimate CH₄ emissions. Section 3 describes the results of the measurements, bias corrections and error estimates, and the best estimates of CH₄ surface emissions implied by the measurements. Section 4 discusses the estimates of CH₄ emissions in the context of current inventories, examines the spatial region in which the tower measurements effectively constrain CH₄ emissions, and concludes with initial recommendations for additional measurement sites to constrain other important emission regions in California.

2. Data and Methods

2.1 CH₄ Measurements

The CH₄ measurements were made at 91 and 483 m on a tall-tower near Walnut Grove, CA (WGC, 121.49 °W, 38.27°N, 0 m above sea level), beginning in September 2007. The measurements were made using a sampling and analysis system combining pumps, air driers, and three gas analyzers. Briefly, air samples are drawn continuously from the different heights on the tower, are partially dried by a condensing system that lowers water vapor to a 5 °C dew point, are sequentially applied on a 5 minute interval to a temperature stabilized membrane drier (Purmapure Inc.) which dries air to a -33 °C dew point, and then are supplied to the gas analyzers. The first 4.5 minutes of each

70 measurement interval are used to allow equilibration of the gas concentrations and
instrument response, while the last 30 seconds is used as the measurement interval. In
particular, CH₄ is measured using a cavity ring-down spectrometer (Picarro EnviroSense
3000i) with an accuracy and precision of approximately 0.3 ppb in the 30 second
75 averaging interval. To quantify and correct instrument drifts, the offset is measured and
corrected every ½ hour using a reference gas, while the gain (and linearity) is checked
and corrected every 6 hours using 4 NOAA gas primary standards. In addition, flask
samples were collected twice daily (1000 and 2200 hr GMT) from a separate sample line
at the 91 m level and analyzed at NOAA-ESRL. To provide additional quality assurance,
the *in-situ* CH₄ measurements were compared with the flask measurements. This
80 redundancy allows the detection of small (~ ppb) sampling errors. In general, the
difference between in-situ and flask analyses was consistent with the precision of the *in-*
situ instrument. During some periods, particularly during late night and early morning,
variability in CH₄ mixing ratios was larger. For these periods, the difference between
flask the *in-situ* CH₄ measurements was generally consistent with the standard deviation
85 of the *in-situ* CH₄ measurements averaged over a 30 minute window centered on the flask
sample.

Fig. 1 shows 3-hour averages of measured CH₄ mixing ratios at 91 m (black) and 483
m (red) in October 2007. Diurnal cycles due to changing boundary layer height are
apparent in the data. The daily maximum CH₄ mixing ratio measured at 91 m often
90 occurs when the minimum is obtained at 483 m. This would be expected to occur in cases
when the boundary layer lies between 91 and 483 m, trapping surface emissions within a
shallow layer that is measured by 91 m sample height, while the 483 m sample height

observes comparatively decoupled background air. In the following work, we will use the daily minimum CH₄ measurements at 483 m to provide a check on the CH₄ background analysis. Moreover, we limited the inverse model study to only include measurements collected during well-mixed periods. Henceforth, we define the well-mixed periods by using the criteria that the difference of measurements at 91 m and 483 m are less than 100 ppb, as shown by the black points in Fig. 1. This criteria will also be evaluated in the following analysis.

100 2.2 Wind Profiler Measurements

To quantify uncertainties in modeled atmospheric transport, hourly boundary layer heights and vertical profiles of winds were obtained from a radar wind profiler (RWP) operated by the Sacramento Metropolitan Air Quality Management District. The profiler is located (38.30°N, 121.42°W) within 8 km of the tower used for the CH₄

105 measurements. Given the level terrain of the Sacramento delta region, we expect that errors in modeled winds and PBL heights for the region surrounding the tower can be accurately assessed by comparing the wind profiler measurements with corresponding meteorological simulations for profiler (winds) and tower (PBL) locations. The RWP acquires data in two different settings, high-resolution and low-resolution mode with vertical resolutions of 60 m and 105 m respectively. Boundary layer heights were estimated from sub-hourly RWP vertical velocity and returned signal strength (signal-to-noise ratio) data using objective algorithms and qualitative analysis following techniques found in *Wyngaard and LeMone* [1980], *Bianco and Wilczak* [2002], and *Bianco et al.* [2008]. In the used configuration, the RWP can detect boundary layer heights from about 115 150 m to 4000 m with an accuracy of ± 200 m [*Dye et al.*, 1995].

2.3 The *a priori* CH₄ Emissions

We used two methods to estimate CH₄ emissions. As a base-case, we used the North American maps of total anthropogenic CH₄ from the EDGAR 3.2 model with 1 x 1 degree spatial resolution [Olivier *et al.*, 2005]. To provide finer spatial resolution inside California, we also estimated California CH₄ emissions separately for six sources sectors: landfills (LF), livestock (LS), natural gas production and use (NG), petroleum refining (PL), crop agriculture (CP), and wetlands (WL). CH₄ emissions from landfills were estimated by the California Air Resources board (Hunsaker, private communication) using IPCC methods [IPCC, 2006], which is driven by landfill specific waste application statistics from the CA Waste Management Board (e.g., Carr, 2004) and site-specific estimates of CH₄ recovery. CH₄ from livestock was estimated using United States Department of Agriculture (USDA) county level animal stocking densities [Census, 2002] and animal specific emission factors for dairy and beef cattle separately [Franco, 2002]. CH₄ from natural gas production and use and from petroleum refining activities were estimated as the difference of total minus reactive hydrocarbon (typically between 0.2-0.4 of the total) emissions estimated from the California Air Resources Board (CARB) emission criteria pollutant emission inventory for those source sectors (<http://www.arb.ca.gov/app/emsinv/fcemssumcat2006.php>). CH₄ emissions from crop agriculture were assumed to follow emissions from the DNDC model for an average climate year with high irrigation as described by Salas *et al.* [2006]. CH₄ emissions from wetlands were assumed to follow the National Aeronautics and Space Administration Carnegie-Ames-Stanford Approach (NASA-CASA) estimates from Potter *et al.* [2006]. Although some of these sources are expected to vary on a seasonal basis, we calculated

mean emissions and did not attempt to resolve temporal variations over the relatively
140 short period of this three months study. Maps of the *a priori* CH₄ emissions are shown in
Figs 2a-f for these six California-specific source sectors. For comparison, Fig. 2g shows
total EDGAR 3.2 emissions for the Western United States, while Fig. 2h shows the sum
of the California-specific CH₄ emissions. Last, Fig. 2i shows a set of California sub-
145 regions that roughly correspond to air basins that are nearby or distant from the
measurement locations and will be used in following analysis. Table 1 summarizes the
CH₄ emissions from different California-specific sources in the 13 sub-regions. CH₄
emissions are scaled to equivalent CO₂ forcing using a global warming potential of 25
(gCO_{2eq} gCH₄⁻¹) [IPCC, 2007]. The total of the California-specific emissions is similar to
150 total CH₄ emissions (~ 31 MMT CO_{2eq}) reported by the California Air Resource Board
[CARB, 2007], but is approximately half the total emissions from California pixels in the
Edgar 3.2 inventory. Inspection of the Edgar 3.2 emissions shows that the largest sources
are from natural gas (22.5 MMT CO_{2eq}) and landfills (19.3 MMT CO_{2eq}), suggesting very
different assumptions about emissions from these sources. To assign an uncertainty to the
a priori emissions, we follow previous work on uncertainty analysis [USEPA, 2004;
155 *Farrell*, 2005] and assign a 30% uncertainty to each of emissions sources. We consider
the uncertainties in US total CH₄ emissions only a rough estimate to the uncertainties for
sub-regions of California (and over the time period of this study) because the 30%
estimate was derived for more aggregated emissions over annual cycles and the entire
continental US.

160 2.4 WRF-STILT Model

As mentioned in the Introduction, the work presented in this paper employs the STILT model, run in the time-reversed (receptor-oriented) mode, as the atmospheric transport model. STILT is a Lagrangian Particle Dispersion Model (LPDM) that has been specifically developed and applied to regional simulations and inverse flux estimates for CO₂, other greenhouse gases, and CO. Its detailed description is provided elsewhere [Lin *et al.*, 2003, 2004; Gerbig *et al.*, 2003a; Matross *et al.*, 2006; Kort *et al.*, 2008; Miller *et al.*, 2008] and, consequently, only the most pertinent features will be summarized here. As in all LPDMs, transport in STILT includes both advective and turbulent components, with turbulence being responsible for the dispersion of particles. In this application, given input meteorological data, the STILT model transports ensembles of 100 particles (air parcels) backwards in time 5 days for a receptor point (WGC site here). We calculate the response of the target gas concentration at the receptor point to surface sources (“footprint”), in units of ppb/(nmol m⁻² s⁻¹). The footprint, which represents the adjoint of the transport field, is calculated by counting the number of particles in a surface-influenced region (defined as ½ of the estimated PBL height in the STILT model, for example see Gerbig *et al.*, 2003a; Kort *et al.*, 2008) and the time spent in the region (for details, see Lin *et al.*, 2003). When multiplied by the *a priori* field of surface flux, the footprint gives the associated contribution to the mixing ratio measured at the receptor, hence the footprints can be used to estimate parameters of the source functions and their respective uncertainties.

We calculate the footprints relating surface fluxes to measured CH₄ mixing ratios using the meteorological output from a customized version of the Weather Research and Forecasting model [Skamarock *et al.*, 2005] to drive STILT. This combined model will

henceforth be referred to as WRF-STILT. Specifically, the WRF model version 2.2 has
 185 been modified to output time-averaged (hourly in this study) values of the mass-coupled
 velocities, which significantly improve mass conservation in STILT (compared with the
 instantaneous advective velocities), as well as convective mass fluxes that are used
 directly in the STILT calculations. The main physical options are set as following: (a)
 Radiation: RRTM scheme [Mlawer *et al.*, 1997] for the longwave and Goddard scheme
 190 [Chou and Suarez, 1994] for the shortwave; (b) Planetary Boundary Layer: Yonsei
 University (YSU) scheme coupled with the NOAH land surface model and the MM5
 similarity theory based surface layer scheme. (c) Microphysics: Purdue Lin scheme [Lin
et al., 1983; Chen and Sun, 2002] (d) Convection: Grell-Devenyi ensemble mass flux
 scheme [Grell and Devenyi, 2002]. The initial and boundary meteorology conditions for
 195 WRF are provided by the North American Regional Reanalysis (NARR, Mesinger *et al.*,
 2006). A one-way nesting WRF running with 3 nest levels is used for the meteorology
 simulations around the WGC tower location, which is shown in Fig. 3 (Domain 1: -
 $149.16^\circ < \text{lon} < -102.21^\circ$, $17.82^\circ < \text{lat} < 50.53^\circ$ on a 40 km grid; Domain 2: $-123.53^\circ <$
 $\text{lon} < -120.66^\circ$, $36.76^\circ < \text{lat} < 38.94^\circ$ on a 8 km grid; Domain 3: $-121.71^\circ < \text{lon} < -$
 200 121.23° , $38.09^\circ < \text{lat} < 38.45^\circ$ on a 1.6 km grid). The vertical resolution is taken from the
 input meteorology from NARR with 30 layers. Each day was simulated separately using
 30-hour run (including 6 hours from the previous day for spin-up) with hourly output.
 Growth in transport model errors were minimized by nudging the forecast fields to the
 gridded NARR analysis fields every 3 hours.

205 2.5 WRF-STILT Transport Errors

As a first approximation to evaluate the transport errors in the WRF-STILT predictions of surface influence footprints, we compared the modeled estimates of WRF winds and WRF-STILT boundary layer heights (Z_i) with corresponding profiler measurements of wind velocity and Z_i . Errors in modeled winds are estimated by comparing WRF predictions with profiler measurements of the u and v wind components at a height of 137m, close to the height of the air sampling. Using data from the October to December 2007, the root mean square (RMS) errors in horizontal winds at 137 m are 2.21 (σ_u) and 2.86 m s^{-1} (σ_v) for the u and v directions respectively. Some of this difference can be attributed to the fact that profiler winds are measured at a single site while the WRF winds are the averages over a grid of 1.6 x 1.6 km. We note that the RMS error decreased by approximately a factor of 2 between 137 m and 1000 m above the ground, though the decrease was non-linear with most of the decrease occurring between 137 and about 500 m. Henceforth, we assume errors in u and v are constant with height and randomly distributed with an RMS magnitude of 3.6 m s^{-1} , which is obtained as

$$\sigma_v = \sqrt{\sigma_u^2 + \sigma_v^2} .$$

Measured and predicted daytime boundary layer heights in October through December 2007 are shown in Fig. 4. Profiler data were selected to match the time of the WRF-predictions to within 1 hour. In addition, the WRF-STILT simulations impose a lower limit value of 215 m on Z_i , while the radar profiler has a minimum detection height of 120 m. To avoid biasing the comparison and make sure CH_4 well mixed from surface till heights above 483 m, we included WRF-STILT predictions of Z_i greater than 215 m in the analysis. The resulting best fit geometric linear regression of WRF-STILT on radar profiler PBL heights yields a slope of 1.25 ± 0.10 and intercept of -138 ± 70 m. Based on

this result, we obtain a scale factor of $1/1.25$ which is then applied to Z_i when calculating
230 footprints using STILT. This result is similar to that found in *Lin et al.* [2003], where
STILT predictions of Z_i were about 1.09 higher than Z_i measurements at a site in
Wisconsin. After scaling STILT Z_i by a factor of $1/1.25$, the RMS residual error between
scaled WRF-STILT and profiler Z_i is reduced by a factor of 1.5 to ~ 200 m, roughly
consistent with the estimated error in the profiler measurements. In the following work
235 we calculate particle trajectories and resulting footprints using the scaled
parameterization of PBL height. It is possible that an additional error in the effective
wind field may be introduced by the Z_i scaling for particles near the top of the boundary
layer if there is significant wind shear at that altitude but expect that this is small
compared to the first order errors already identified for winds and PBL heights.

240 2.6 Footprints and Predicted CH₄ Signals

Particle trajectories were calculated using STILT driven by the WRF winds. One
hundred particles are released every 3 hours (from UTC hour 00) at the WGC tower and
transported backward in time 5 days to insure a majority of the particles reach positions
representative of the marine boundary layer. Footprints are then calculated from the
245 particle trajectories as in *Lin et al.* [2004]. The time-averaged footprint is shown in Fig. 5
for the period between October and December in 2007. The high footprint values within
approximately the Central California area near the tower site indicate that CH₄ signals
measured at 91 m and 483 m at WGC will be strongly influenced by the California
emissions.

250 Predicted local CH₄ signals $C_l(\underline{X}_r, t_r)$ (index ‘l’ denote local and ‘r’ denote receptor)
 from land surface emissions are calculated using the product of the footprint maps and
 the *a priori* emission maps, as

$$C_l(\underline{X}_r, t_r) = \sum_{i,j,m} f(\underline{X}_r, t_r | x_i, y_j, t_m) \cdot F(x_i, y_j) \quad (1)$$

, where \underline{X}_r and t_r are receptor (WGC tower) location and time, $f(\underline{X}_r, t_r | \underline{X}, t_m)$ is the
 255 footprint and $F(x_i, y_j)$ is the surface emission map at location (x_i, y_j) and time t_m . The
 total CH₄ mixing ratio at the receptor can be expressed as

$$C(\underline{X}_r, t_r) = C_l(\underline{X}_r, t_r) + C_{BG}(\underline{X}_r, t_r) \quad (2)$$

, where $C_{BG}(\underline{X}_r, t_r)$ is the upstream CH₄ background mixing ratios.

2.7 Inversion Technique

260 The *posterior* CH₄ emissions were estimated by optimizing scaling factors for the *a*
priori CH₄ emissions to provide a best fit between measured and predicted CH₄ mixing
 ratios. This was done in two ways: 1) as a standard least square optimization of an overall
 scaling factor for all land surface emissions and 2) in a Bayesian approach that scales
 each source type or sub-region separately and incorporates individual estimates for the
 265 uncertainties in different *a priori* emissions.

Combining Eq. (1) and (2), the difference between measured and predicted
 background CH₄ relates to the surface emission flux as

$$\underline{C} - \underline{C}_{BG} = \underline{fF}, \quad (3)$$

where \underline{f} is footprints, \underline{F} is surface CH₄ emission, \underline{C} and \underline{C}_{BG} is CH₄ mixing ratios from
 270 tower measurements and background calculations, respectively. Assuming mixing ratio

measurements from local sources as $y = \underline{C} - \underline{C}_{BG}$. Following *Gerbig et al.* [2003a], we introduce a model parameter or a state vector of scaling factors, $\underline{\lambda}$, for the surface flux, $\underline{F}(\underline{\lambda})$. The inversion adjusts the model parameters $\underline{\lambda}$ such that the modeled changes in CH₄ concentrations are optimally consistent (in standard least square sense) with the observed values. In the study of surface CH₄ emissions from different sources (“source analysis” hereafter), $\underline{\lambda}$ represents the scaling factor for different sources; in the study of surface CH₄ emissions from different regions (“region analysis” hereafter), $\underline{\lambda}$ represents the scaling factor for different areas. For both the “source analysis” and “region analysis” study, $\underline{F}(\underline{\lambda})$ is linearly dependent on $\underline{\lambda}$:

$$\underline{F}(\underline{\lambda}) = \underline{\phi}\underline{\lambda} \quad (4)$$

where $\underline{\phi}$ is the *a priori* emissions for different sources or regions in this study.

Using the same method as *Lin et al.* [2004], the analytical solutions to Eqs (3) and (4) are

$$\begin{aligned} \hat{\underline{\lambda}} &= (\underline{K}^T \underline{S}_{\varepsilon}^{-1} \underline{K})^{-1} (\underline{K}^T \underline{S}_{\varepsilon}^{-1} \underline{y} + \underline{S}_{prior}^{-1} \underline{\lambda}_{prior}) \\ \hat{\underline{S}}_{\underline{\lambda}} &= (\underline{K}^T \underline{S}_{\varepsilon}^{-1} \underline{K} + \underline{S}_{prior}^{-1})^{-1} \end{aligned} \quad (5)$$

where $\underline{K} = \underline{f}\underline{\phi}$, $\underline{S}_{\varepsilon}$ is measurement error covariance matrix $\underline{\lambda}_{prior}$ and $\hat{\underline{\lambda}}$ are the *a priori* and *a posteriori* vectors, and \underline{S}_{prior} and $\hat{\underline{S}}_{\underline{\lambda}}$ are the *a priori* and *a posteriori* error matrices for $\underline{\lambda}$. Corresponding to our initial estimate of 30% uncertainty in the CH₄ emission maps, the initial value of \underline{S}_{prior} is 0.09. Note that the measurements and *a priori* emission error matrices are diagonal, equivalent to assuming that the prior errors are uncorrelated. The measured and predicted CH₄ signals are computed and compared on a 3 hour interval.

2.8 Error Covariance Matrix

The equivalent “measurement” error covariance matrix S_ε is formed as the sum of different components

$$\underline{S}_\varepsilon = \underline{S}_{part} + \underline{S}_{aggr} + \underline{S}_{TransWND} + \underline{S}_{TransPBL} + \underline{S}_{bkgd} + \underline{S}_{eddy} + \underline{S}_{ocean} \quad (6)$$

295 Here, as in *Lin et al.* [2004], the contribution of instrumentation error in the CH₄ measurements is assumed to be random, uncorrelated, and negligible in magnitude relative to the other sources of error, and hence not considered further in the inverse model estimates. We consider each of the terms in Eq. (6) below.

The particle number error (S_{part}) is due to the finite number of released particles at
 300 the receptor location. It can be estimated by comparing the simulated signals from the STILT running with release of 1000 particles and those from the STILT running with release of 100 particles. Using the WRF simulated meteorology in October 2007 and the total *a priori* emission map, we found that the standard error is about 3 ppb, indicating ~5% particle number error. This value is less than ~13% particle number error for CO₂
 305 indicated by *Gerbig et al.* [2003a]. Considering the ~5% error determined by us here and ~13% error determined by *Gerbig et al.* for signals in the mixed-layer, S_{part} for 100 particles is assumed as 10% in this study. For all of the following error analyses, we used 1000 particles in order to minimize the effect of particle number error.

The “aggregation error” (S_{aggr}) arises from aggregating heterogeneous fluxes within a
 310 grid cell into a single average flux [*Kaminski et al.*, 2001]. *Gerbig et al.* [2003b] demonstrated that a rough estimate of the aggregation error can be derived from the observed “representation error”, which is derived from the difference between a point

observation and a value averaged over a specific grid size [Gerbig *et al.*, 2003a].

Without multiple observation stations over a specific grid, we try to estimate the
 315 aggregation error based on the *a priori* CH₄ emissions. Although we do not have high-
 resolution emission maps for all of the CH₄ sources, we estimate aggregation error using
 landfill emissions, which are fully resolved. Here, the aggregation error is estimated by
 comparing the un-aggregated landfill signal from to the landfill signal estimated after
 averaging emissions over each county (the maximum aggregation used for the other
 320 sources). The average aggregation error, estimated as the RMS difference between the
 un-aggregated and aggregated signals, is 11% of the mean landfill signal.

The transport error ($S_{\underline{Trans}} = S_{\underline{TransWND}} + S_{\underline{TransPBL}}$) denotes the errors in modeling
 transport, which can be caused by the uncertainties in wind speeds and directions, and the
 uncertainties in PBL heights. Following Lin and Gerbig [2005], the transport error due to
 325 winds $S_{\underline{TransWND}}$ is calculated as the RMS difference between signals predicted from
 simulations with and without input of an additional stochastic component of wind error
 σ_V (3.6 m/s; Section 2.5) in STILT. The resulting RMS signal is equivalent to 8% of the
 average predicted CH₄ signal. This estimate of uncertainty assumes that the wind error at
 the radar profiler location can be used to represent the wind error within the modeling
 330 domain. While we have not evaluated the wind errors for other locations, we note that the
 3.6 m/s wind error used here is comparable to the mean wind error of 3.08 m/s,
 determined from radiosonde observations over the coterminous U.S. between 0 and 3 km
 in altitude [Lin and Gerbig, 2005].

Uncertainty due to errors in modeled PBL heights S_{TransPBL} is estimated by

335 propagating the residual error Z_i into the predicted CH_4 signals. Here, we use the estimate of residual error in Z_i determined from the comparison between predicted WRF-STILT PBL height and PBL height measured with the wind profiler. The sensitivity of CH_4 signal to Z_i is expressed as a first order perturbation in C as

$$\gamma = \frac{dC}{dZ_i} \quad (7)$$

340 where γ is estimated by calculating STILT footprints and then variations in C for small perturbations in Z_i . The error due to error in Z_i can then be estimated as

$$S_{\text{transPBL}} = \frac{\Delta C}{\langle C \rangle} = \frac{\gamma \cdot \Delta Z_i}{\langle C \rangle} \quad (8)$$

where ΔZ_i is the residual error in WRF-STILT Z_i , and $\langle C \rangle$ is the mean total CH_4 signal.

Note that this error is calculated for well-mixed conditions. Using Eqs. (7) and (8), the

345 estimated transport error due to PBL uncertainties is 22% of the mean signal.

The background error (S_{bkgd}) is due to the uncertainty in estimating the background

contribution to the CH_4 measurements at WGC 91 m. For this study, we estimate the

upstream background CH_4 mixing ratio using the final latitude of each particle as a

lookup into the latitudinally averaged marine boundary layer (MBL) CH_4 for October-

350 December, 2007 (NOAA Globalview CH_4). Only time points (> 95% of the total) for

which more than 80% of the particles reached longitudes 1.5 degrees from the coast were

included in the study. We expect that the NOAA MBL average will be a reasonable

approximation for the CH_4 background because it is heavily weighted to the Pacific and

the typical CH_4 gradients between Pacific and Atlantic are less than 10 ppb. We

355 evaluated the error in CH_4 background using the daily minimum CH_4 mixing ratio

measured at 483 m. The reason that the daily minimum CH₄ mixing ratio at 483m often reflects that of background air is because the 483m sample height decouples from the surface at night (when $91 \text{ m} < Z_i < 483 \text{ m}$) as indicated in Fig. 1. A comparison of the CH₄ mixing ratios determined from the NOAA MBL average and WGC 483m minimum estimates is shown as a function of time in Fig 6. Fig 6 (b) shows that there is no systematic bias, although the minimum CH₄ mixing ratio at 483 m is occasionally enhanced relative to the NOAA MBL average, likely due to local CH₄ contributions. We estimate the error due to CH₄ background as the RMS difference in Fig 6 (b), which is 15% of the mean background-subtracted measurements at 91 m.

The eddy flux error (S_{eddy}) specifies the fluctuations in CH₄ mixing ratios due to contributions from turbulent eddies. *Gerbig et al.* [2003a] observed it is ~ 0.2 ppm for CO₂. For CH₄ studied here, a value of 1% is assumed. The error due to omitting ocean emissions (S_{ocean}) is assumed to be negligible. To evaluate this assumption, we calculated the expected CH₄ signal from the Coal Point field near Santa Barbara, the largest known coastal natural gas field near California [*Mau et al.*, 2007], and found the signals to be less than 1 ppb.

In order to combine the above errors from different sources, we need to know their correlations, which are unfortunately unknown. Assuming the errors from different sources are independent, the above errors are combined in quadrature to yield a total expected model-prediction mismatch error of 32%.

3. Results

3.1 CH₄ Mixing Ratios

Predicted CH₄ signals and background-subtracted measurements at 91 m are shown in Fig. 7. As described in sections 2.1 and 2.8, data are selected to only include times with well-mixed conditions and when background CH₄ can be reliably, which are shown as black points in Fig. 7. Diurnal cycles due to changing boundary layer height and synoptic variations due to frontal passages are apparent in the data. The data gap in early-mid December resulted from a leak in the sampling system that was diagnosed and repaired. The measured and predicted CH₄ mixing ratios show similar temporal variations, indicating partial success of the model. However, the predicted signals do not always capture the large CH₄ measurements, indicating some combination of errors in the *a priori* emission model (e.g., spatial pattern or limited resolution) and atmospheric transport (e.g, wind fields, boundary layer height).

3.2 Inferred Surface Emissions

We compare the tower measurements and WRF-STILT simulations at WGC site during winter (October-December) 2007. Three analyses are reported here: 1) a linear analysis for total CH₄ emissions; 2) a “source analysis” for the six CH₄ source sectors; and 3) a “region analysis” for thirteen regions in CA. For the linear analysis, we employ a Chi-square linear regression analysis by assuming equal relative errors of 32% in both variables. For the “source analysis” and “region analysis”, the Bayesian analysis from Eqs. (7) and (8) is applied. Note that the “region analysis” used the same *a priori* spatial distributions of CH₄ emissions as the “source analysis”, and same total effective measurement errors of 32% are used in the following analyses.

3.2.1 Linear Regression Analysis

400 Results of the regression analyses using California specific emission applied to the
October through December 2007 period are shown in Figs. 8a and 8b. Without Z_i scaling
(Fig. 8a), the best-fit slope between predicted and measured CH_4 mixing ratios is $0.46 \pm$
 0.07 . After applying the Z_i scaling to WRF-STILT (Fig. 8b), the slope between predicted
and measured CH_4 is 0.73 ± 0.11 . The change in slope between Fig. 8a and Fig. 8b
405 demonstrates that scaling the PBL heights affects the predicted CH_4 signals, and any
residual uncertainty in PBL height should be considered as a source of uncertainty in the
Bayesian analyses that follow. After the Z_i scaling, the slope obtained in Fig. 8b suggests
that the actual emissions are higher than inventory estimates by a factor of 1.37 ± 0.21 .
We note that the normalized Chi-square value for Fig. 8b is 1.17, suggesting that the
410 estimated errors do not completely explain the residual variance in the differences
between the predictions and measurements. CH_4 signals based on Edgar 3.2 emissions are
also simulated and compared with the tower measurements in Fig. 8c, yielding a slope of
 1.09 ± 0.14 . This slope is roughly consistent ($p > 0.1$ in a t test) with the slope ($0.92 \pm$
 0.03) obtained by *Kort et al.* [2008] in their comparison of measured and predicted CH_4
415 signals using Edgar 3.2. However, the slopes obtained with the California specific (Fig.
8b) and Edgar (Fig. 8c) emissions are significantly different ($p < 0.01$), as might be
expected given the large difference in the *a priori* emissions shown in Table 1. For the
central California region, the total emission estimated by Edgar 3.2 is about 75% more
than that estimated from California specific sources, which is roughly consistent with the
420 difference ($\sim 50\%$) of fitting slopes between Fig. 8b and Fig. 8c.

To evaluate the effect of the well-mixed data selection criteria, we also examined the slopes obtained with a more stringent requirement that the difference between CH₄ mixing ratio measured at 91 m and 483 m is less than 50 ppb. This subset of data are shown as triangles in Fig. 8. Using the selection criteria of 50 ppb in Fig. 8) obtains a slope of 0.86 ± 0.17 , which is quite consistent with that obtained using the selection criteria of 100 ppb. The following analyses include data based on the 100 ppb selection criteria.

3.2.2 Bayesian Analysis

The Bayesian “source” inverse analysis was carried out for the six source sectors for October through December 2007. As shown in Fig. 9 (a), the *a posteriori* scaling factors for the crop agriculture (CP), landfill (LF), wetland (WL), petroleum (PL), and natural gas (NG) are not significantly different from unity (at 95 % confidence). The scaling factor for livestock is 1.63 ± 0.22 , suggesting the emissions from livestock are significantly (95% confidence) larger than the *a priori* inventory estimates. The Bayesian “region” inverse analysis of emissions from the 13 California regions is shown in Fig. 9(b). The *a posteriori* uncertainties are noticeably reduced relative to the *a priori* uncertainties only for regions 6, 7, and 8, which have a strong influence on the CH₄ measurements either because the land surrounds the tower site (regions 6 and 8) or has a tele-connection through the prevailing wind (region 7). The *a posteriori* scaling factor for region 6 is 1.08 ± 0.06 , indicating that the posterior emissions agree well with the *a priori* inventory estimates. Posterior scaling factors for region 7 and 8 are 1.55 ± 0.17 and 1.37 ± 0.15 respectively, indicating that the *a posteriori* emissions are greater than the *a priori* estimates for these two regions.

445 After applying the scaling factors obtained from Bayesian analyses, the posterior
predicted CH₄ mixing ratios are compared with measurements in Fig. 10. Fig. 10a shows
the comparison for results from the ‘source analysis’ with measurements. Compared to
Figure 8b (before inverse optimization), the fitting slope is closer to unity, and the
normalized Chi-square value is slightly reduced from 1.17 to 1.11. This suggests that the
450 inverse optimization has slightly improved the agreement between the measured and
predicted CH₄ signals but that on order 10% of the variance remains unexplained. It is
possible that the apparent underestimation of the errors may be due to positive correlation
between the error sources that we assumed independent. Similar results are obtained for
the region analysis, as shown in Fig. 10b. In both cases, the slopes after optimization are
455 still slightly less than unity, likely because of the weight on the *a priori* scaling factors.
We note that relaxing the *a priori* uncertainties on the scaling factors from 30% to 50%,
allows the optimization to adjust the posterior scaling factors further from their *a priori*
values.

4. Discussion and Conclusions

460 Here we discuss the impact of error in PBL height on uncertainty in estimated CH₄
emissions, the implications of our results on estimated CH₄ emissions from Central
California, and conclude with recommendations for additional measurement sites that
would help quantify CH₄ emissions from more regions in California.

465 First, the results of this work highlight the need for careful estimation and
minimization of errors in the transport model. Our work is really only a first step in this
regard because we have only evaluated wind and PBL height errors for one site, albeit at
the location where the CH₄ measurements were made. The comparison between the radar

profiler measurements and WRF-STILT predictions of PBL height show a systematic
470 overestimation in the WRF-STILT predictions, while the sensitivity test shows that
predicted CH₄ emission estimates are sensitive to PBL height. The error in WRF-STILT
predictions of PBL height may be a result of imperfect land surface parameterization in
WRF that does not account for a suppression of PBL height in the Central Valley.
Possible causes for overestimation of PBL height include the Pacific low over
475 California's interior and low ratios of sensible to latent heat (Bowen ratios) driven by
agricultural irrigation as shown in recent model studies of California [Kueppers *et al.*,
2007; Lobel and Bonfils, 2008]. Because of the limited amount of PBL height data, the
present work should be considered a first step toward a more comprehensive analysis
employing profiler data from additional profiler sites and over longer periods. We expect
480 that this effort will substantially improve the fidelity of the WRF-STILT PBL predictions
and hence accuracy of GHG emission inversions.

Second, the linear regression estimates suggest that October-December CH₄
emissions from Central California are estimated to be 37 ± 21 % higher than the annually
averaged California specific *a priori* inventories. Examining the source sector results, the
485 increase in overall emissions is largely due to the 63 ± 22 (1 σ) % increase in estimated
emissions from livestock. State-wide *a priori* livestock emission are 9.7 MMT CO_{2eq} (see
Table 1), which includes 5.6 MMT CO_{2eq} from dairies and 4.1 MMT CO_{2eq} from other
cattle. Scaling the *a priori* CH₄ emissions from dairies suggests that actual dairy
emissions are 9.1 ± 1.3 MMT CO_{2eq}. This result is nominally consistent with or slightly
490 less than the results of a recent study by Salas *et al.* [2008], which estimated total CH₄
emissions from dairies in CA to be approximately 9.8 MMT CO_{2eq}. We note that the

source sector and regional analyses are consistent with each other in that CH₄ emission from region 8, which is dominated by livestock, shows a large and statistically significant increase relative to the *a priori* inventory. Some other sources also showed smaller but not significant differences from inventory estimates. For example, inferred CH₄ emissions from crop agriculture are smaller than the annually averaged inventory, consistent to the expectation of higher CH₄ emissions from the north-central Valley during the summer due to flooded rice agriculture [Salas *et al.*, 2006]. Finally, the “region” analysis shows that emissions from regions 6, 7 and 8 are constrained by the measurements. This is because they either surround the tower (i.e., regions 6 and 8) or have a strong influence on air reaching the tower through prevailing winds from the Bay Area to the Sacramento Valley (i.e., region 7). This observation provides an insight into the spatial domain that can be effectively investigated with the tower measurements and suggests that a network of towers would be required to accurately constrain the multiple regions and air basins in California. In principle, measurements from multiple towers would also be combined in a larger inverse analysis to provide more stringent constraints on emissions from regions that influence several towers. We consider a model-based design of a dedicated tower network to be a natural extension of the work described here.

Acknowledgements

510 We thank Dave Field, Dave Bush, Edward Wahl, and particularly Jon Kofler for
assistance with installation and maintenance of the instrumentation at WGC, Edward
Dlugokencky for advice and assistance in verifying the Picarro instrument performance at
NOAA, John Lin and Steve Wofsy for generously sharing the STILT code and providing
expert advice, Chris Potter and William Salas for sharing their models of CH₄ emission
515 for use as *a priori* estimates, Larry Hunsaker and Webster Tassat for providing the
CARB estimates of landfill CH₄ emissions, Ken Massarie for providing the global CH₄
background data, and Susan James for assistance running WRF on the LBNL-ASD
computer cluster. We gratefully acknowledge NOAA Air Resources Laboratory (ARL)
for the use of the HPSPLIT model underlying STILT, and NCEP for the provision of the
520 NARR meteorology. We also thank Jean Bogner, Nancy Brown, Eric Crosson, Guido
Franco, Ling Jin, Ying-Kuang Hsu, Eileen McCauley, Tony VanCuren, James Wilczack,
and three anonymous reviewers for valuable comments. This study was supported by the
California Energy Commission (CEC) Public Interest Environmental Research Program
and the Director, Office of Science, Office of Basic Energy Sciences, of the U.S.
525 Department of Energy under Contract No. DE-AC02-05CH11231. The findings, views,
and opinions presented in this paper do not necessarily represent the views and opinions
of the California Energy Commission or the State of California.

References

- Bergamaschi, P., M. Braunlich, T. Marik, and C. A. M. Brenninkmeijer (2000), Measurements of the carbon and hydrogen isotopes of atmospheric methane at Izana, Tenerife: Seasonal cycles and synoptic-scale variations, *J. Geophys. Res.*, **105**(D11), 14531-14546.
- Bergamaschi, P., M. Krol, F. Dentener, A. Vermeulen, F. Meinhardt, R. Graul, M. Ramonet, W. Peters, and E. J. Dlugokencky (2005), Inverse modeling of national and European CH₄ emissions using the atmospheric zoom model TM5, *Atmos. Chem. Phys.*, **5**, 2431-2460.
- Bergamaschi, P., et al. (2007), Satellite cartography of atmospheric methane from SCIAMACHY on board ENVISAT: 2. Evaluation based on inverse model simulations, *J. Geophys. Res.*, 112, D02304, doi:10.1029/2006JD007268.
- Bianco, L., and J. M. Wilczak (2002), Convective boundary layer depth: improved measurement by Doppler radar wind profiler using fuzzy logic methods. *J. Atmos. Ocean. Technol.* **19**(11), 1745-1758.
- Bianco, L., J. M. Wilczak, and A. B. White (2008), Convective boundary layer depth estimation from wind profilers: Statistical comparison between an automated algorithm and expert estimations, *J. Atmos. Ocean. Tech.*, **25**, 1397-1413.
- CARB (2007), California 1990 Greenhouse Gas Emissions Level and 2020 Emissions Limit. California Air Resources Board Staff Report.
(http://www.arb.ca.gov/cc/inventory/pubs/reports/staff_report_1990_level.pdf)

- Carr, N. (2004), Overall Waste Stream Composition Data. California Integrated Waste Management Board: 1999 California Statewide Waste Disposal Characterization Study. (<http://www.ciwmb.ca.gov/WasteChar/Study1999/OverTab1.htm>).
- Census of Agriculture 2002 - Volume 1 California County Level Data. National Agricultural Statistical Services for U.S. Agriculture Statistical Information and Graphs. United States Department of Agriculture. (<http://www.nass.usda.gov/census/census02/volume1/ca/index2.htm>).
- Chen, Y.-H., and R. G. Prinn (2006), Estimation of atmospheric methane emissions between 1996 and 2001 using a three-dimensional global chemical transport model, *J. Geophys. Res.*, 111, D10307, doi:10.1029/2005JD006058.
- Chen S.-H., and W.-Y. Sun (2002), A one-dimensional time dependent cloud model. *J. Meteor. Soc. Japan*, **80**, 99–118.
- Chou, M.-D., and M. J. Suarez (1994), An efficient thermal infrared radiation parameterization for use in general circulation models. *NASA/TM-104606*, **10**, 84pp.
- Dentener, F., W. Peters, M. Krol, M. van Weele, P. Bergamaschi, and J. Lelieveld (2003), Inter-annual-variability and trend of CH₄ lifetime as a measure for OH changes in the 1979-1993 time period, *J. Geophys. Res.*, **108**(D15), 442, doi: 10.1029/2002JD002916.
- Dye, T.S., C. G. Lindsey, and J. A. Anderson (1995), Estimates of mixing depth from “boundary layer” radar profilers. *Preprints from the 9th Symposium on Meteorological Observations and Instrumentation*, Charlotte, NC, March 27-31, 156-160 (STI-94212-1451).

- Franco, G. (2002). Inventory of California Greenhouse Gas Emissions and Sinks: 1990-1999. California Energy Commission: Public Interest Energy Research. (CEC-600-02-001F).
- Farrell, A., Kerr, A.C., Brandt, A.R., Torn, M.S., and G. Franco (2005). Research Roadmap for Greenhouse Gas Inventory Methods. California Energy Commission: Public Interest Energy Research. (CEC-500-2005-097)
- Gerbig C., J. C. Lin, S. C. Wofsy, B. C. Daube, A. E. Andrews, B. B. Stephens, P. S. Bakwin, and C. A. Grainger (2003a), Toward constraining regional-scale fluxes of CO₂ with atmospheric observations over a continent: 1. Observed spatial variability from airborne platforms, *J. Geophys. Res.*, **108** (D24), 4756, doi:10.1029/2002JD003018.
- Gerbig, C., J. C. Lin, S. C. Wofsy, B. C. Daube, A. E. Andrews, B. B. Stephens, P. S. Bakwin, and C. A. Grainger (2003b), Toward constraining regional-scale fluxes of CO₂ with atmospheric observations over a continent: 2. Analysis of COBRA data using a receptor-oriented framework, *J. Geophys. Res.*, **108** (D24), 4757, doi:10.1029/2003JD003770.
- Gimson, N. R. and Uliasz, M. (2003), The determination of agricultural methane emissions in New Zealand using receptor-oriented modelling techniques. *Atmos. Environ.*, **37**, 3903-3912.
- Grell, G.A. and D. Devenyi (2002), A generalized approach to parameterizing convection combining ensemble and data assimilation techniques, *Geoph. Res. Lett.*, **29**(14), 10.1029/2002GL015311.

- Hansen, J., Mki. Sato, J. Glascoe, and R. Ruedy, 1998: A common sense climate index: Is climate changing noticeably? *Proc. Natl. Acad. Sci.*, **95**, 4113-4120.
- Hansen, J., 2004: Defusing the global warming time bomb. *Sci. Amer.*, **290**(3), 68-77.
- Harriss, R.C. (1994), Reducing urban sources of methane: an experiment in industrial ecology. *Industrial Ecology and Global Change*, Cambridge Univ. Press, 223-238.
- Hein, R., P. J. Crutzen, and M. Heimann (1997), An inverse modeling approach to investigate the global atmospheric methane cycle. *Global Biogeochemical Cycles* **11**(1), 43–76.
- Hofman, D. J., J. H. Butler, E. J. Dlugokencky, J. W. Elkins, K. Masarie, S. A. Montzka, and P. Tans, (2006): The role of carbon dioxide in climate forcing from 1979 - 2004: Introduction of the Annual Greenhouse Gas Index, *Tellus B*, **58B**, 614-619.
- Houweling, S., T. Kaminski, F. Dentener, J. Lelieveld, and M. Heimann (1999), Inverse modeling of methane sources and sinks using the adjoint of a global transport model. *J. Geophys. Res.*, **104**(D21), 26137-26160.
- Houweling, S., T. Röckmann, I. Aben, F. Keppler, M. Krol, J. F. Meirink, E. J. Dlugokencky, and C. Frankenberg (2006), Atmospheric constraints on global emissions of methane from plants, *Geophys. Res. Lett.*, **33**, L15821, doi:10.1029/2006GL026162.
- IPCC (2006) Guidelines for National Greenhouse Gas Inventories (<http://www.ipcc-nggip.iges.or.jp/public/2006gl/index.htm>)
- IPCC (2007), IPCC Fourth Assessment Report (AR4), “Climate Change 2007”.

- Kaminski, T., P. J. Rayner, M. Heimann, and I. G. Enting (2001), On aggregation errors in atmospheric transport inversions, *J. Geophys. Res.*, **106**(D5), 4703–4715.
- Kort, E. A., J. Eluszkiewicz, B. B. Stephens, J. B. Miller, C. Gerbig, T. Nehrkorn, B. C. Daube, J. O. Kaplan, S. Houweling, and S. C. Wofsy (2008), Emissions of CH₄ and N₂O over the United States and Canada based on a receptor-oriented modeling framework and COBRA-NA atmospheric observations, *Geophys. Res. Lett.*, **35**, L18808, doi:10.1029/2008GL034031.
- Kueppers, L. M., M. A. Snyder, and L. C. Sloan, (2007), Irrigation cooling effect: Regional climate forcing by land-use change. *Geophys. Res. Lett.*, **34**, L03703, doi:10.1029/2006GL028679.
- Lelieveld, J., P. J. Crutzen, and F. J. Dentener (1998), Changing concentration, lifetime, and climate forcing of atmospheric methane, *Tellus B*, **50**, 128-150.
- Lin Y.-L., R. D. Farley, and H. D. Orville (1983), Bulk parameterization of the snow field in a cloud model. *J. Appl. Meteor.*, **22**, 1065–1092.
- Lin, J. C., and C. Gerbig (2005), Accounting for the effect of transport errors on tracer inversions, *Geophys. Res. Lett.* **32**, L01802, doi:10.1029/2004GL021127.
- Lin, J. C., C. Gerbig, S. C. Wofsy, A. E. Andrews, B. C. Daube, C. A. Brainger, B. B. Stephens, P. S. Bakwin, and D. Y. Hollinger (2004), Measuring fluxes of trace gases at regional scales by Lagrangian observations: Application to the CO₂ Budget and Rectification Airborne (COBRA) study. *J. Geophys. Res.* **109**, D15304, doi:10.1029/2004JD004754.
- Lin, J. C., C. Gerbig, S. C. Wofsy, A. E. Andrews, B. C. Daube, K. J. Davis, and C. A. Grainger (2003), A near-field tool for simulating the upstream influence of

- atmospheric observations: The Stochastic Time-Inverted Lagrangian Transport (STILT) model, *J. Geophys. Res.*, **108**(D16), 4493, doi:10.1029/2002JD003161.
- Lobel, D.B., C. Bonfils, (2008) The Effect of Irrigation on Regional Temperatures: A Spatial and Temporal Analysis of Trends in California, 1934–2002. *J. of Climate*, **21**, 2063.
- Manning, A. J., D. B. Ryall, R. G. Derwent, P. G. Simmonds, and S. O’Doherty (2003), Estimating European emissions of ozone-depleting and greenhouse gases using observations and a modeling back-attribution technique, *J. Geophys. Res.*, **108** (D14), 4405, doi: 10.1029/2002JD002312.
- Matross, D. M., A. Andrews, M. Pathmathevan, C. Gerbig, J. C. Lin, S. C. Wofsy, B. C. Daube, E. W. Gottlieb, V. Y. Chow, J. T. Lee, C. Zhao, P. S. Bakwin, J. W. Munger, and D. Y. Hollinger (2006), Estimating regional carbon exchange in New England and Quebec by combining atmospheric, ground-based and satellite data, *Tellus B*, **58**, 344-358.
- Mau, S., D. L. Valentine, J. F. Clark, J. Reed, R. Camilli, and L. Washburn (2007), Dissolved methane distributions and air-sea flux in the plume of a massive seep field, Coal Oil Point, California, *Geophys. Res. Lett.*, **34**, L22603.
- Mesinger, F., G. DiMego, E. Kalnay, K. Mitchell, P. C. Shafran, W. Ebisuzaki, D. Jovic, J. Woollen, E. Rogers, E. H. Berbery, M. B. Ek, Y. Fan, R. Grumbine, W. Higgins, H. Li, Y. Lin, G. Manikin, D. Parrish, and W. Shi (2006), North America Regional Reanalysis, *Bull. Amer. Meteor. Soc.*, **87** (3), 343-360.
- Mikaloff Fletcher, S. E., P. P. Trans, L. M. Bruhwiler, J. B. Miller, and M. Heimann (2004a), CH₄ sources estimated from atmospheric observations of CH₄ and its

- $^{13}\text{C}/^{12}\text{C}$ isotopic ratios: 1. Inverse modeling of source processes, *Global Biogeochem. Cycles*, **18**, doi: 10.1029/2004GB002223.
- Mikaloff Fletcher, S. E., P. P. Tans, L. M. Bruhwiler, J. B. Miller, and M. Heimann (2004b), CH_4 sources estimated from atmospheric observations of CH_4 and its $^{13}\text{C}/^{12}\text{C}$ isotopic ratios: 2. Inverse modeling of CH_4 fluxes from geographical regions, *Global Biogeochem. Cycles*, **18**, doi: 10.1029/2004GB002224
- Miller, J. B., and P. P. Tans (2003), Calculating isotopic fractionation from atmospheric measurements at various scales, *Tellus B*, **55**(2), 207-214.
- Miller, S. M., D. M. Matross, A. E. Andrews, D. B. Millet, M. Longo, E. W. Gottlieb, A. I. Hirsch, C. Gerbig, J. C. Lin, B. C. Daube, R. C. Hudman, P. L. S. Dias, V. Y. Chow, and S. C. Wofsy (2008), Sources of carbon monoxide and formaldehyde in North America determined from high-resolution atmospheric data, *Atmos. Chem. Phys.*, **8**, 7673-7696.
- Mlawer, E. J., S. J. Taubman, P. D. Brown, M. J. Iacona, and S. A. Clough (1997), Radiative transfer for inhomogeneous atmospheres: RRTM, a validated correlated-k model for the longwave, *J. Geophys. Res.*, **102**, 16663-16682.
- Olivier, J. G. J., J. A. Van Aardenne, F. Dentener, L. Ganzeveld, and J. A. H. W. Peters (2005), Recent trends in global greenhouse gas emissions: regional trends and spatial distribution of key sources. In: “*Non-CO₂ Greenhouse Gases (NGGG-4)*”, 325-330. Millpress, Rotterdam, ISBN 90 5966043 9.
- Potter, C., S. Klooster, S. Hiatt, M. Fladeland, V. Genovese and P. Gross (2006), Methane Emissions from Natural Wetlands in the United States: Satellite-Derived Estimation Based on Ecosystem Carbon Cycling. *Earth Interactions*, **10**, 1–12.

- Salas, W., P. Green, S. Frolking, C. Li and S. Boles (2006). Estimating Irrigation Water Use for California Agriculture: 1950s to Present. California Energy Commission, PIER Energy-Related Environmental Research. CEC-500-2006-057.
- Salas, W., Li, C., Mitloehner, F., and J. Pisano (2008). Developing and Applying Process-based Models for Estimating GHG and Air Emission from California Dairies. California Energy Commission, PIER Energy-Related Environmental Research. CEC-500-2008-XXX (in press).
- Skamarock, W. C., J. B. Klemp, J. Dudhia, D. O. Gill, and D. M. Barker, and W. Wang, and J. G. Powers (2005), A description of the advanced research WRF version 2. Technical Note 468+STR, MMM Division, NCAR, Boulder, CO, 88 p.
- Shindell, D. T., G. Faluvegi, N. Bell, and G. A. Schmidt (2005), An emissions based view of climate forcing by methane and tropospheric ozone, *Geophys. Res. Lett.*, **32**, L04803, doi:10.1029/2004GL021900.
- USEPA, (2004), *Inventory of U.S. Greenhouse Gas Emissions and Sinks: 1990–2002*. Washington D.C., U.S. Environmental Protection Agency, April 15, 2004. EPA 430-R-04-003.
- Vermeulen, A. T., R. Eisma, A. Hensen, and J. Slanina (1999), Transport model calculations of NW-European methane emissions, *Environ. Sci. Policy*, **2**, 315-324.
- Wyngaard, J.C., and M. A. LeMone (1980), Behavior of the refractive index structure parameter in the entraining convective boundary layer. *J. Atmos. Sci.* **37**,1573-1585.

LBNL, MS 90K

1 Cyclotron Rd.

Berkeley, CA 94720

czhao@lbl.gov

Figure Captions

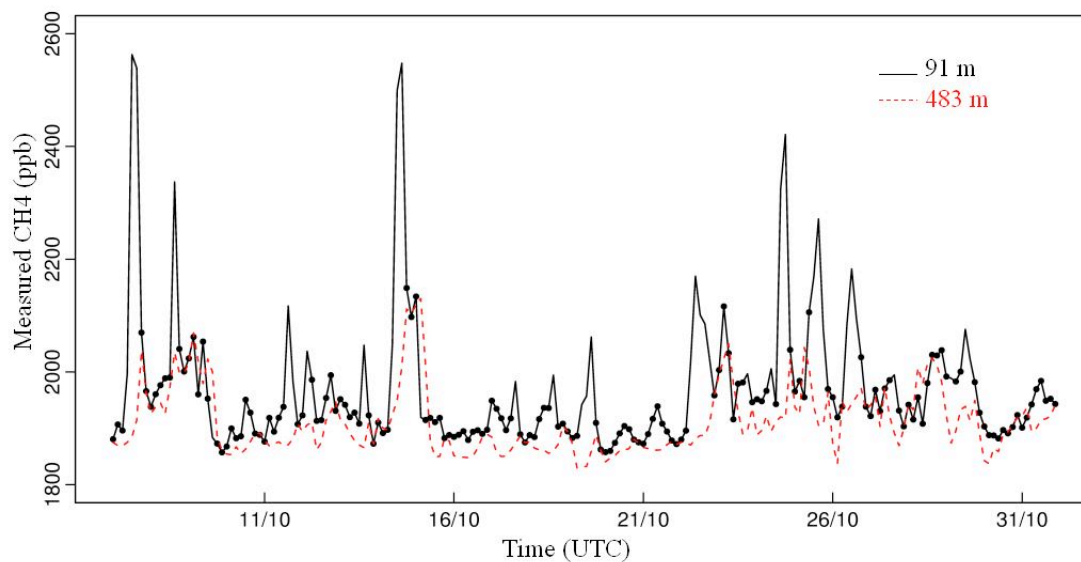


Figure 1. CH₄ mixing ratios measured at 91 m (black) and 483 m (red) at the WGC tower. Only data (black points) obtained during well-mixed periods (defined as when the difference between measurements at 91 m and 483 m are less than 100 ppb) are used in this study.

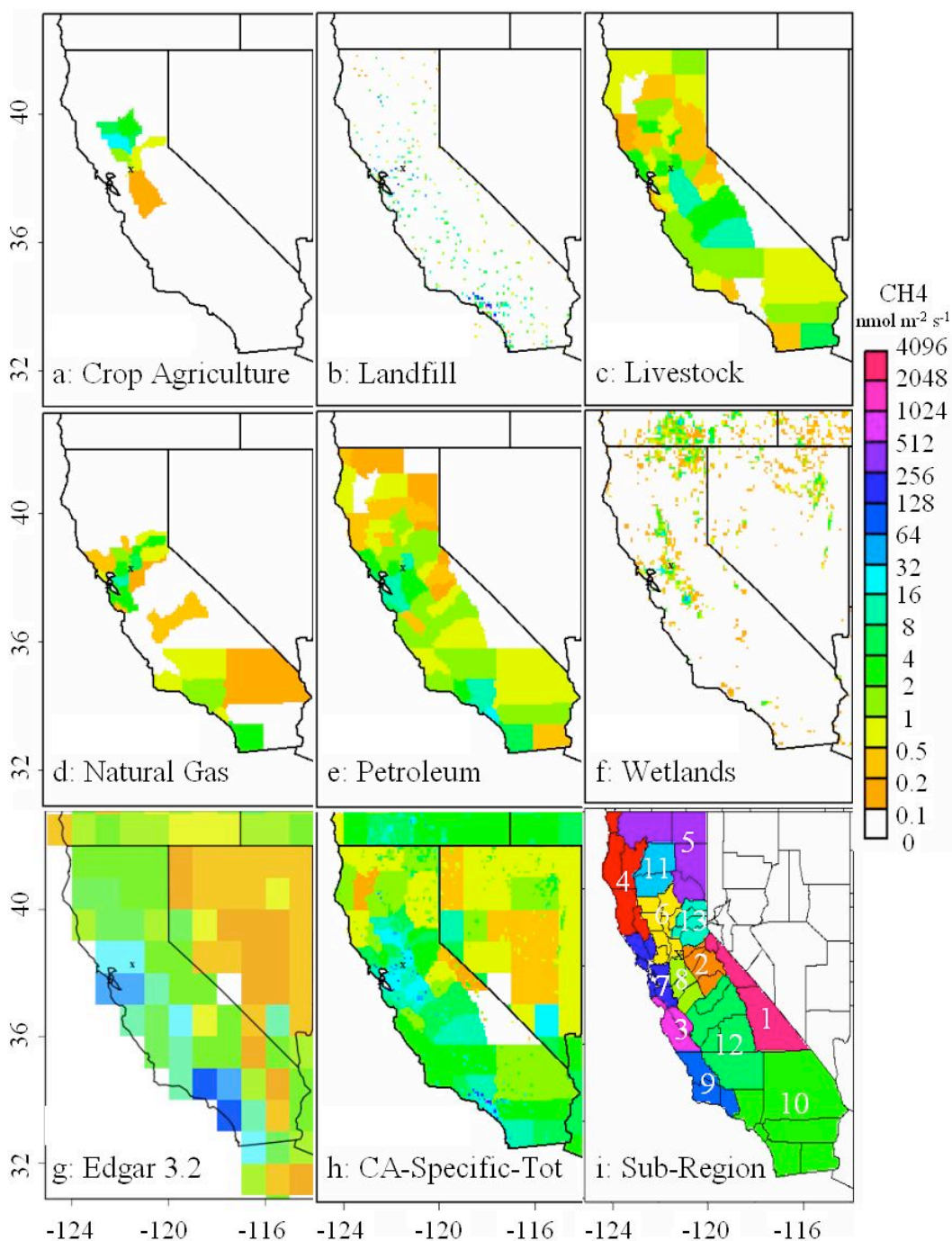


Figure 2. The *a priori* emission maps and regions in California. a-f) are the CA-specific surface CH₄ emissions from different sources; g) is anthropogenic surface CH₄ emissions from Edgar 3.2; h) is the sum of maps a-f) specific to California; and i) is an illustration of the 13 California sub-regions considered in the region analysis. The tower location is marked with a 'x'.

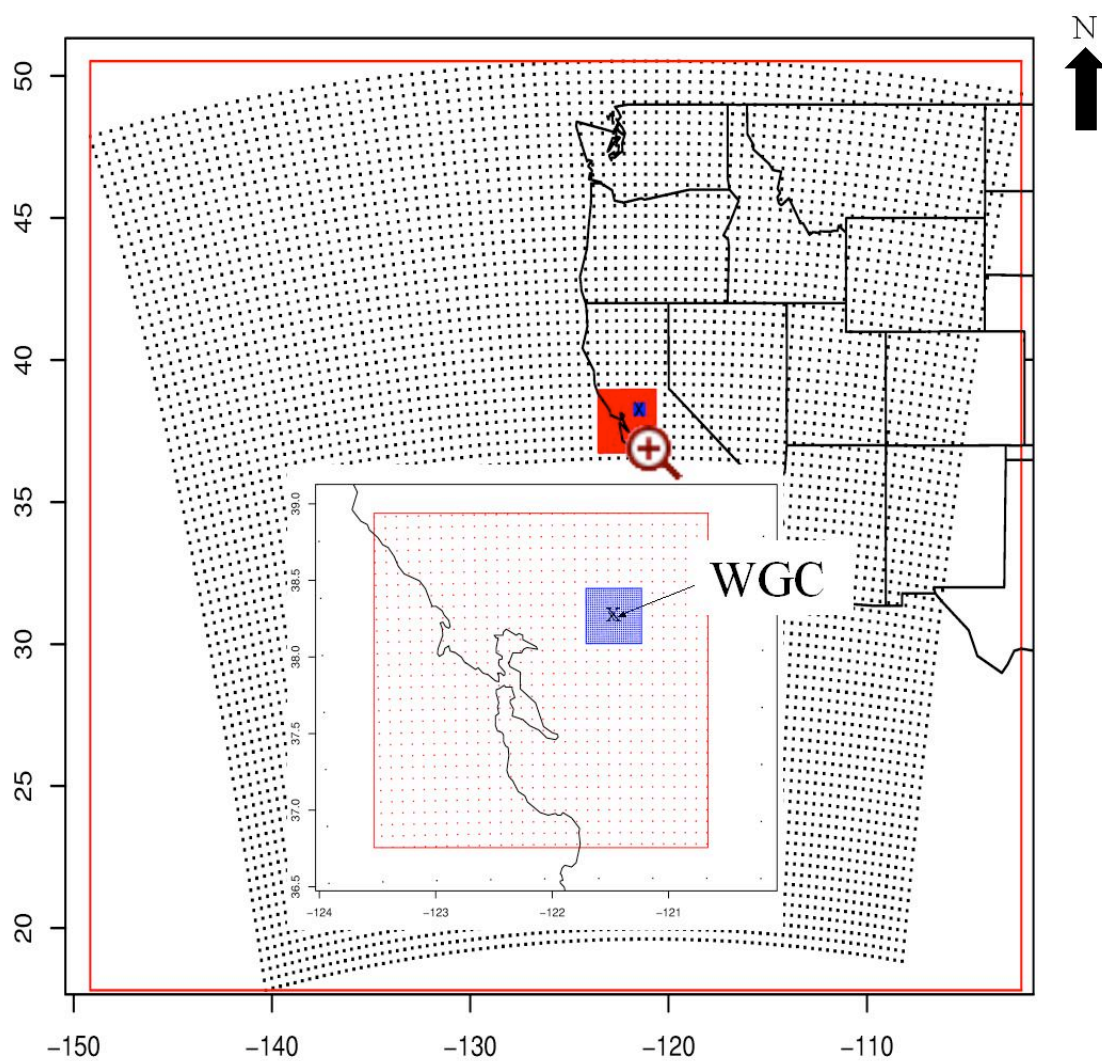


Figure 3. Map grids showing the three model domains used in the meteorological predictions, and WGC tower location “X” (-121.49, 38.26) of the measurements.

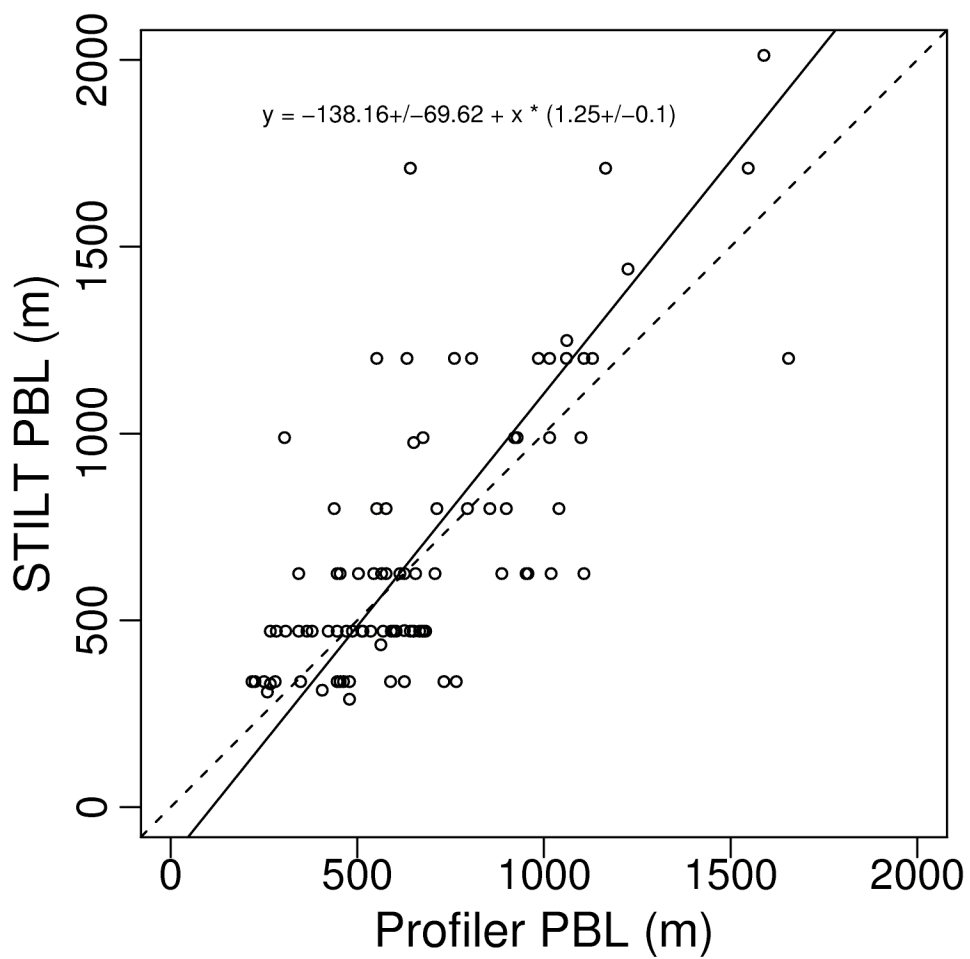


Figure 4. Comparison of well-mixed daytime PBL heights between radar profiler measurements and WRF-STILT simulations in October through December 2007.

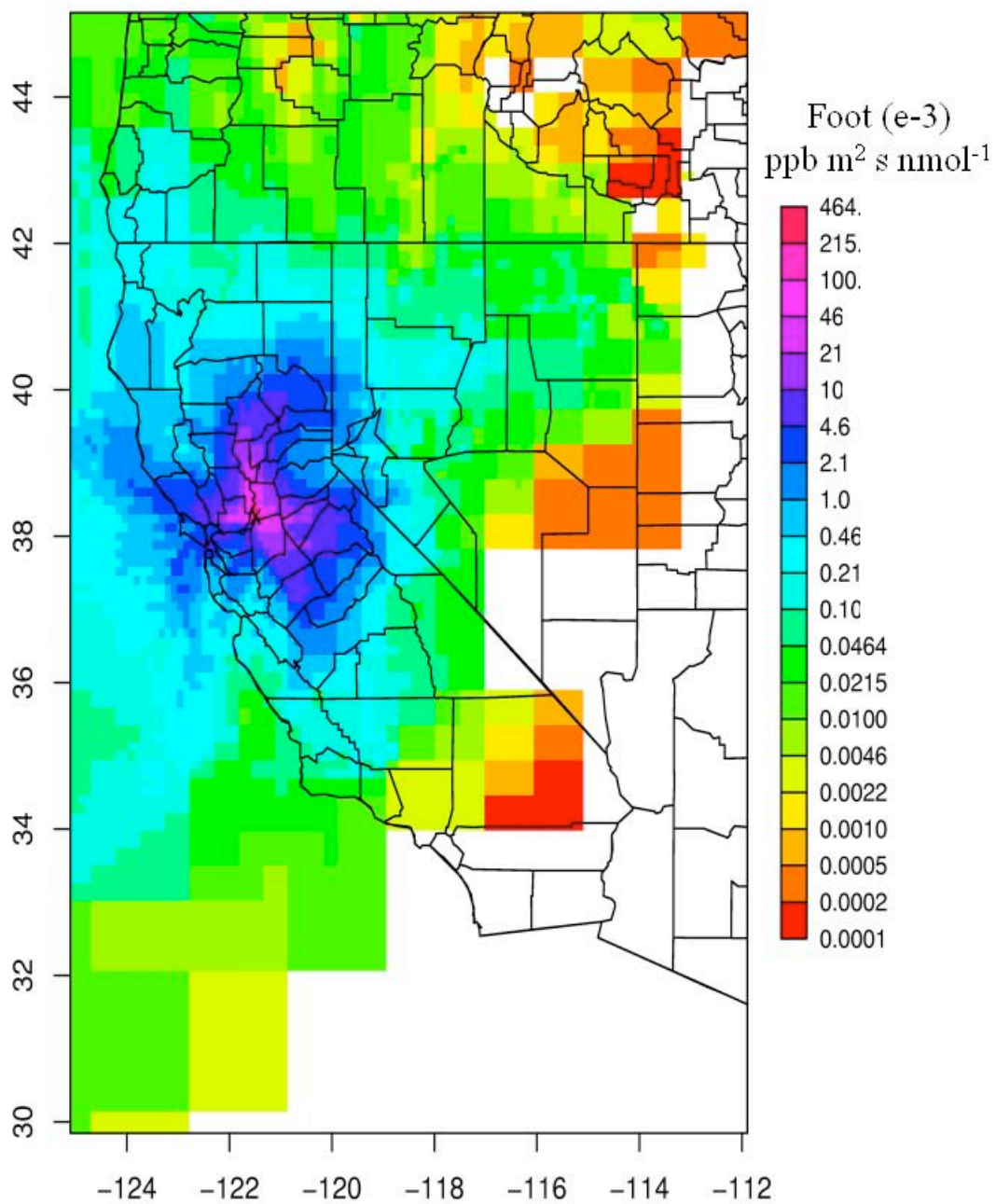


Figure 5. Averaged footprints for mixing ratio measurements made at the tower location 'X' (-121.49, 38.26).

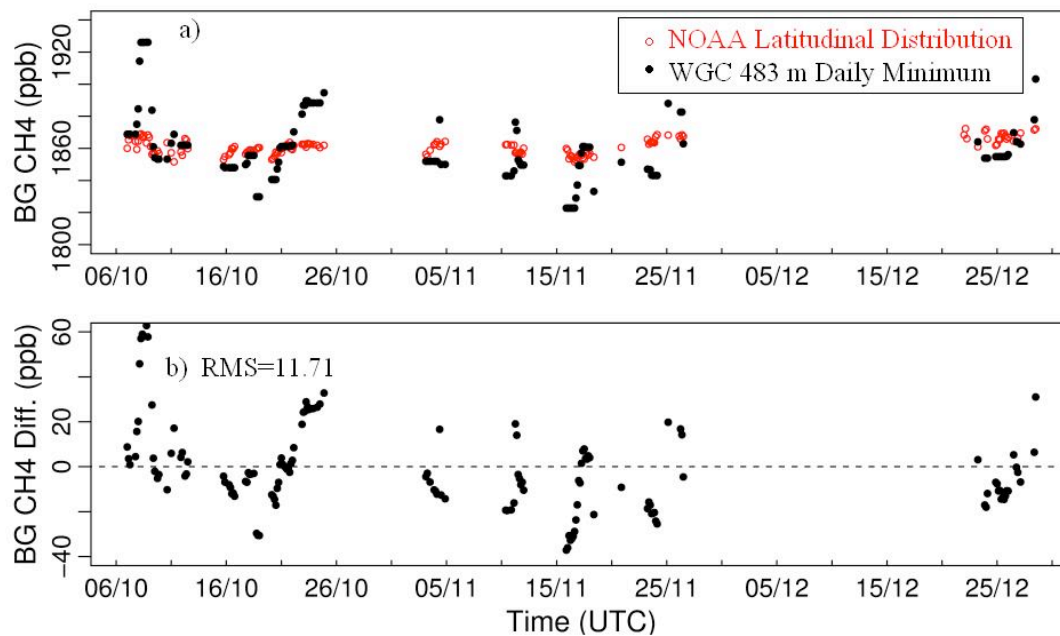


Figure 6. Time series of background CH₄ mixing ratios, calculated from the NOAA global latitudinal average marine boundary layer (red) and the daily minimum measured at 483 m (black) a), and the difference of these signals b).

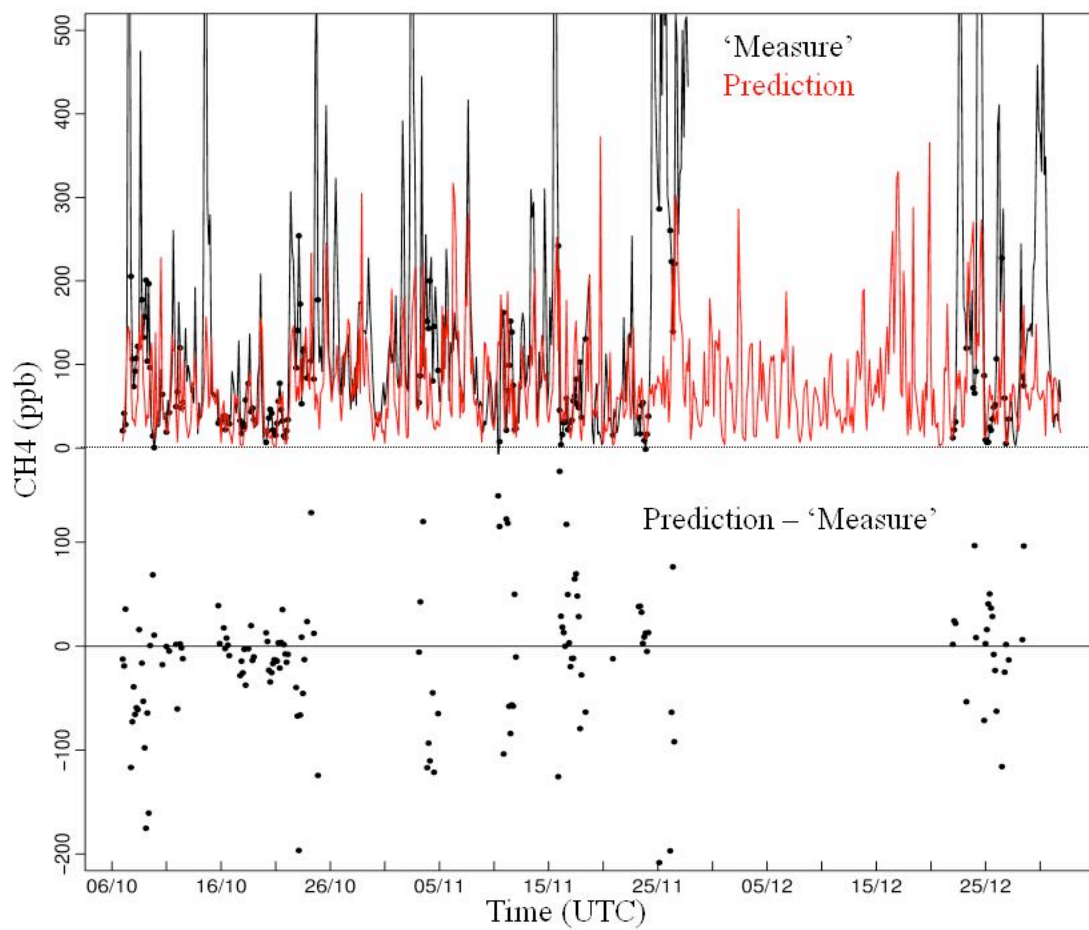


Figure 7. Background subtracted CH₄ measurements (black line) and predictions (red line) from 91 m as a function of time (top), and their difference (bottom) for well mixed conditions (black points).

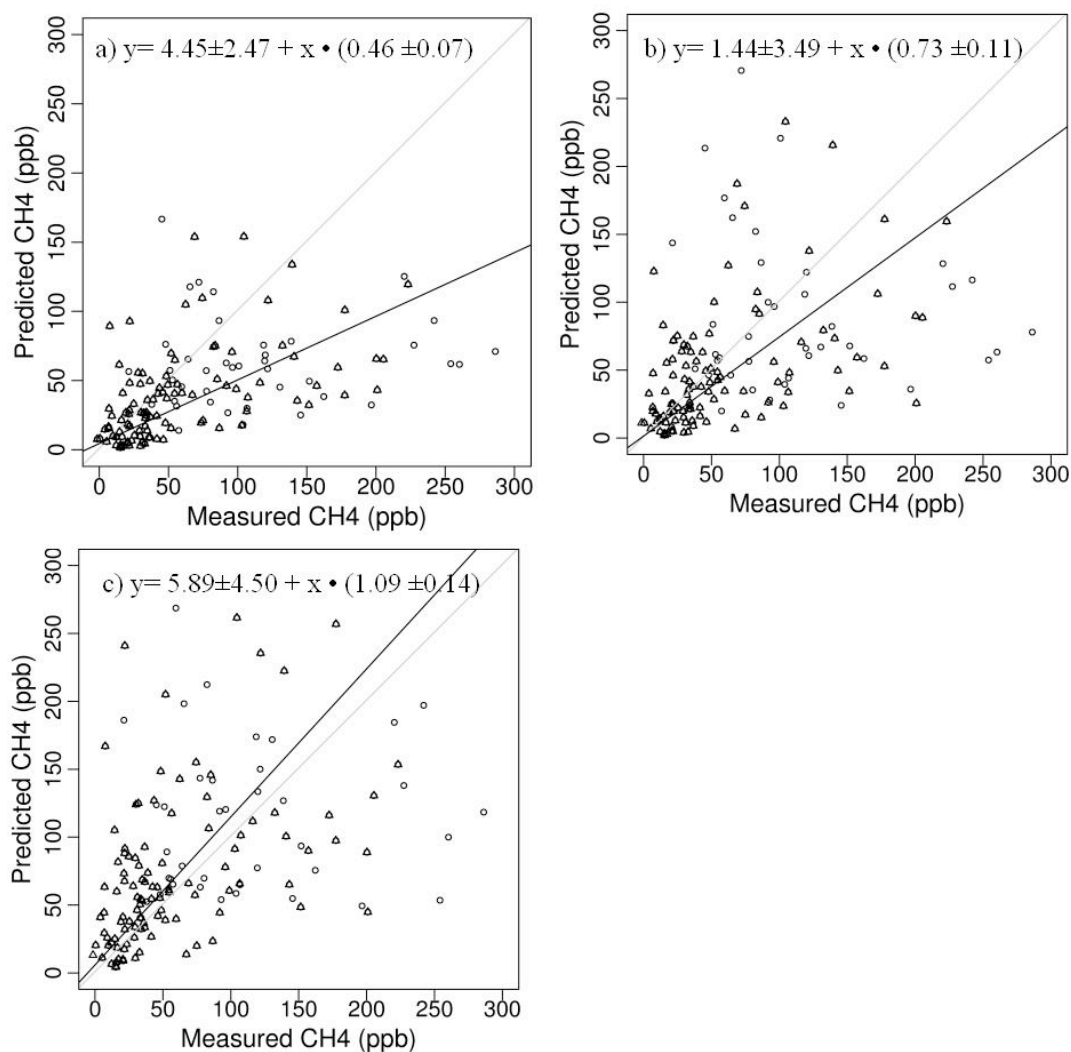


Figure 8. Predicted versus measured CH₄ obtained (a) using California specific emissions without Z_i correction, (b) with Z_i correction, and (c) using Edgar 3.2 emissions with Z_i correction. The symbols indicate well-mixed periods when the difference between CH₄ mixing ratios measured at 91 and 483 m are less than 100 ppb (open circles) and less than 50 ppb (triangles), respectively.

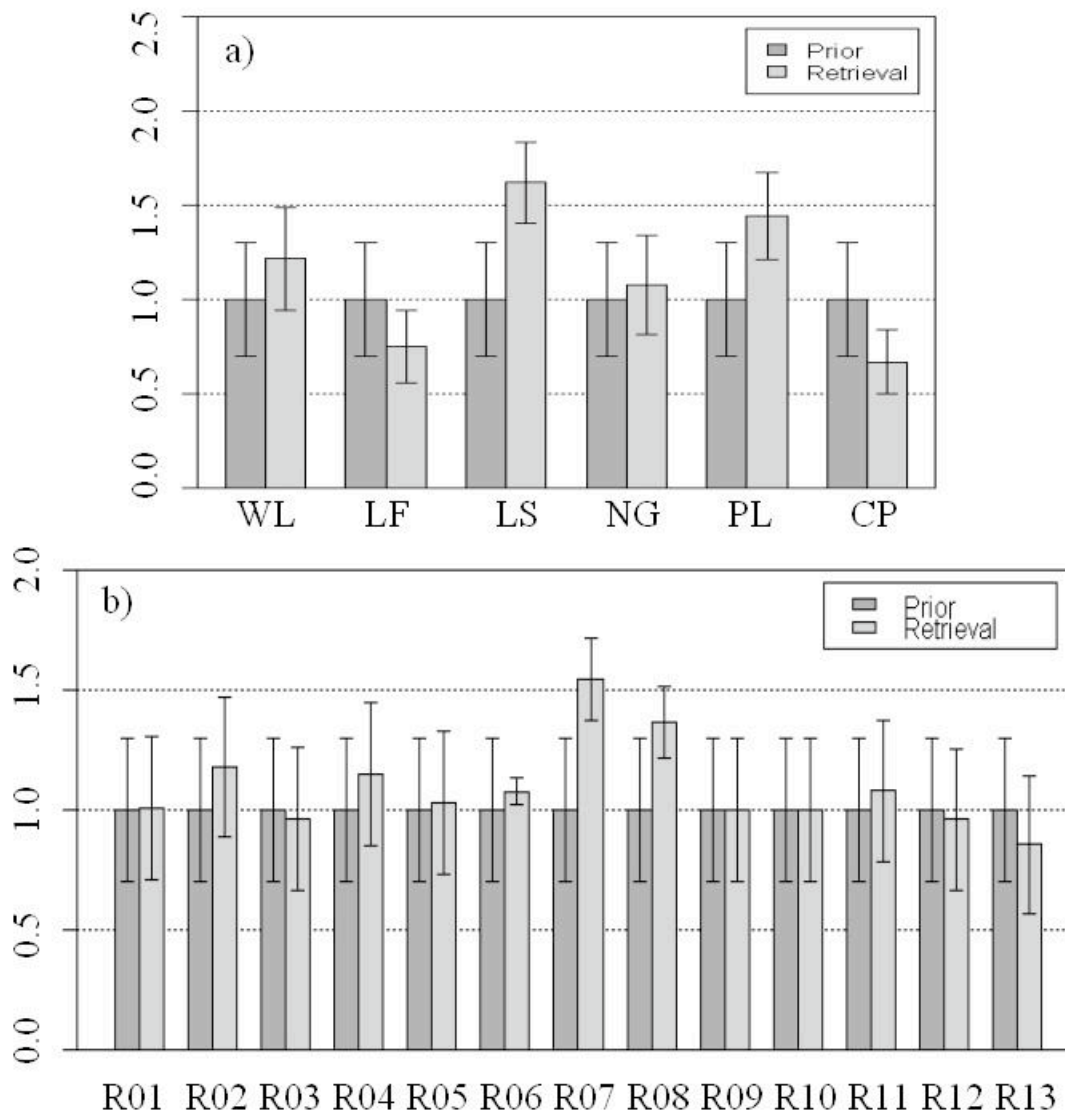


Figure 9. Inversion estimates for the “source” sector analysis (a) and “region” analysis (b). *A priori* and *posterior* scaling factors for the six source sectors and 13 source regions are shown with corresponding 68% confidence level uncertainties.

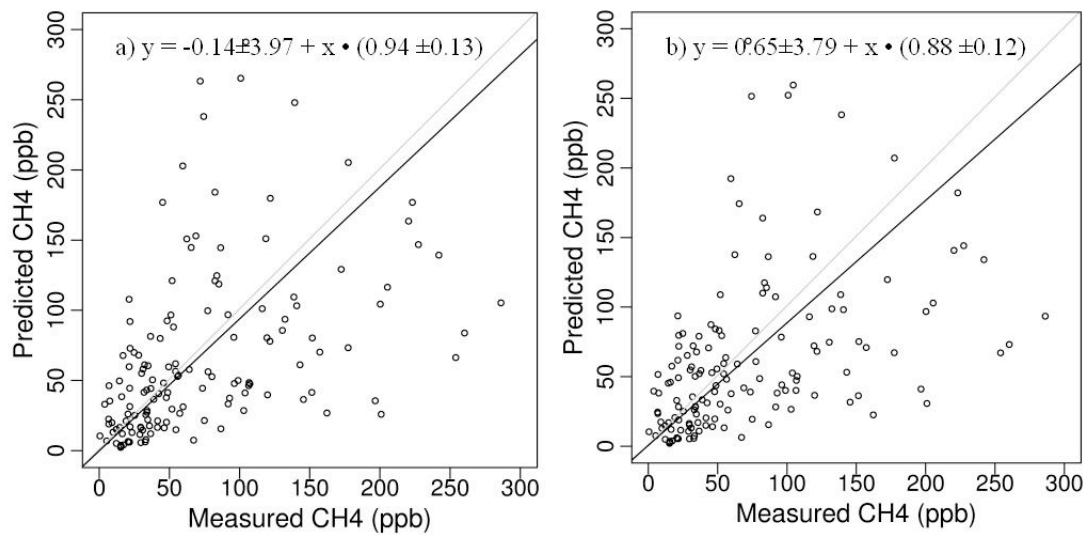


Figure 10. Comparison of CH₄ mixing ratios between measurements and predictions modified using posterior scaling factors obtained from the “source” analysis (a) and “region” analysis (b).

Tables

Table 1. *A priori* CH₄ emissions (MMT CO_{2eq}) from 6 different sources and 13

California regions shown in Figure 2i.

CH ₄ (MMT CO _{2eq})	CP	LF	LS	NG	PL	WL	CA.spec	Edgar3.2
Region 01	0.04	0.02	0.04	0.00	0.02	0.06	0.18	0.92
Region 02	0.01	0.04	0.15	0.00	0.10	0.02	0.29	1.09
Region 03	0.01	0.05	0.20	0.01	0.20	0.02	0.45	1.74
Region 04	0.04	0.10	0.18	0.00	0.17	0.05	0.48	1.56
Region 05	0.05	0.02	0.39	0.00	0.11	0.07	0.57	1.76
Region 06	0.02	0.40	0.51	0.36	0.62	0.04	1.81	4.30
Region 07	0.01	0.74	0.31	0.67	1.50	0.02	3.25	5.95
Region 08	0.01	0.27	2.06	0.01	0.32	0.02	2.32	3.73
Region 09	0.02	0.26	0.24	0.13	0.37	0.02	0.96	3.48
Region 10	0.11	3.75	1.68	0.88	3.62	0.17	10.21	25.14
Region 11	0.02	0.13	0.19	0.01	0.10	0.02	0.47	1.09
Region 12	0.06	0.31	3.65	0.31	0.73	0.10	5.16	7.95
Region 13	0.01	0.06	0.06	0.19	0.19	0.02	0.53	1.07
Whole CA	0.42	6.15	9.66	2.57	8.03	0.63	27.46	59.78